Diagnosing the Annual Cycle of the Equatorial Undercurrent in the Atlantic Ocean from a General Circulation Model

Michel Arhan, Anne-Marie Tréguier, B. Bourlès, S. Michel

Diagnosing the Annual Cycle of the Equatorial Undercurrent in the Atlantic Ocean from a General Circulation Model

M. ARHAN AND A. M. TREGUIER

Laboratoire de Physique des Océans, CNRS/IFREMER/UBO, Brest, France

B. BOURLÈS

Centre IRD de Brest, Brest, France

S. MICHEL

Laboratoire de Physique des Océans, CNRS/IFREMER/UBO, Brest, France

(Manuscript received 22 September 2004, in final form 3 January 2006)

ABSTRACT

Ten-year-long output series from a general circulation model forced by daily realistic winds are used to analyze the annual cycle of the Equatorial Undercurrent (EUC) in the Atlantic Ocean. Two well-defined transport maxima are found: One, present during boreal summer and autumn in the central part of the basin, is generally recognized and regarded as a near-equilibrium response to the equatorial easterly trades that culminate in this period. Another one, most pronounced near the western boundary, occurs in April–May when the trades relax. This second maximum is less patent in the observations, but concomitant signals in previously published analyses of the North Brazil Current and surface velocity seasonal variations might be indirect manifestations of its reality. Because this intensification appears at periods when the boundary between the tropical and equatorial gyres nears the equator, the authors relate its existence to wind stress curl variations at subequatorial latitudes. A link between the interannual variability of the spring transport maximum and that of the low-latitude wind stress curl is, indeed, found in the model. This diagnostic approach suggests that two different dynamical regimes shape up the EUC seasonal cycle: in summer and autumn, local forcing by the equatorial zonal wind component and main supply from the ocean interior; in winter and spring, remote forcing by the low-latitude rotational wind component and supply from the western boundary currents.

1. Introduction

Although the response of the upper equatorial Atlantic Ocean to the low-latitude seasonal wind regime has been well described and understood for the most part, that of the Equatorial Undercurrent (EUC) remains uncertain. Contrary to nonequatorial currents, whose variability is reflected in variations of the meridional slopes of isopycnals [see Garzoli and Katz (1983) for the North Equatorial Countercurrent (NECC)], and at variance with equatorial surface currents directly inferred from the drifts of surface buoys or ships (Richardson and McKee 1984), the EUC cumulates the observational difficulties associated with nongeostrophic, subsurface, and jetlike flows.

As early as the 1970s, the difficulty of simply relating the intensity of the undercurrent to that of the local wind was noted by Philander (1973), and Katz et al. (1977) observed from an analysis of Global Atmospheric Research Program (GARP) Atlantic Tropical Experiment (GATE) measurements that, while the equatorial zonal pressure gradient was strongly correlated to the simultaneous wind stress, no such relation exists between these variables and the undercurrent mass transport. Data analyses in the 1980s underlined a well-defined seasonal heaving of the undercurrent but confirmed a more confused transport variability. Katz et al. (1981), using observations between 25° and 33°W from the Global Weather Experiment, found the high-

Corresponding author address: M. Arhan, LPO, IFREMER/Centre de Brest, 29280 Plouzané, France.
E-mail: michel.arhan@ifremer.fr

est EUC transport [an isolated estimate of 43.5 Sv (Sv $\equiv 10^6$ m^3 s^{-1})] in northern spring when the equatorial easterly wind component is weakest and found a secondary maximum (26 Sv) in August when the easterlies have intensified. Hisard and Hénin (1987) found the highest of eight EUC transport estimates obtained at 23°W, during the Program Français Océan et Climat dans l'Atlantique Equatorial/Seasonal Response of the Equatorial Atlantic (FOCAL/SEQUAL) experiment, in autumn when the westward wind stress and zonal pressure gradient at 50 db were most intense. Weisberg et al. (1987), from 2.7-yr current time series at 0°, 28°W, observed no replicating annual cycle of the EUC transport, a revelation of an interannual variability which constitutes an additional hindrance to the detection of seasonal effects. In the last 15 years, measurements of the EUC velocities by shipborne acoustic Doppler current profilers (ADCPs) have provided many new estimates of the undercurrent transport. However, both interannual and intraseasonal variabilities have so far prevented the establishment of a clear annual cycle of the EUC from these observed snapshot transports (Schott et al. 1998; Stramma and Schott 1999).

While these observational efforts were being made, the time-variable dynamics of the EUC have also been analyzed in model studies. Katz and Garzoli (1982), using a theoretical model with an on/off steady uniform zonal wind, managed to qualitatively reproduce the spring intensification suggested by the observations of Katz et al. (1977). Using a linear model forced by monthly averaged climatological winds, du Penhoat and Treguier (1985) found a single broad maximum of the EUC transport most pronounced at 20°–30°W in September, in equilibrium with the wind stress forcing. The primitive equation model of Philander and Pacanowski (1986a) shows two EUC zonal velocity extrema at 30°W, one in April–May and a second one in October–December—the latter producing the highest transport (Philander and Pacanowski 1986b). The same two maxima of the EUC transport are present in subsequent model results (Schott and Böning 1991; Hazeleger et al. 2003). Following process studies of Philander and Pacanowski (1980, 1981), the autumn maximum is generally regarded as an equilibrium response to the concomitant extremum of the easterly trades that set the eastward pressure gradient. Although Katz and Garzoli (1982) regarded the spring maximum as a possible response to sudden winter relaxations of the wind, there has been, up to now, some disregard for this feature less evidently related to the equatorial zonal wind.

The idea that wind forcing at nonequatorial latitudes should also influence the EUC was put forward by Pedlosky (1987, 1988, 1996) in a stationary theory that regards the undercurrent as an inertial equatorial boundary flow extending the ventilated thermocline flow solution of the subtropics (Luyten et al. 1983). The ensuing question of *remote* versus *local* forcing of the EUC and the determination of possible communication pathways from higher latitudes were discussed in several studies of the so-called subtropical cells (STC) that connect the subtropics to the equator (McCreary and Lu 1994; Liu 1994; Liu et al. 1994), and of which the EUC is the eastward limb. A set of general circulation model experiments led Liu and Philander (1995) to conclude that, although most of the EUC water comes from the subtropics, the transport of the current is mainly determined by the winds in the Tropics. The simplified tropical wind stress patterns specified by Liu and Philander were, however, stationary and purely zonal so that they provide no information on how the low-latitude realistic winds affect the EUC transport variability. Some studies on the STCs did address the question of the seasonal variability (Lazar et al. 2002), but they focused on variations of the subtropical–tropical connection rather than on the EUC cycle.

Considering the observational difficulties mentioned above, realistic models still provide a useful tool to analyze the EUC annual cycle. This holds particularly as model resolutions fitted to the equatorial jetlike structures are now available, as are pluriannual model forcings whose variability may help to recognize cause-and-effect relationships. This is the approach proposed in this study, which is focused on the description and understanding of the annual cycle of a model Atlantic EUC. Section 2 presents the model and compares its time-averaged EUC with observations. Section 3 describes the annual cycle of the model undercurrent characterized by maxima in spring (autumn), at periods when the equatorial easterly trades are lowest (highest). In section 4 we discuss observational signs of the spring maximum in the literature. The outlines of a possible dynamical interpretation of the spring maximum are presented in section 5 and discussed in section 6, before the study is concluded in section 7.

2. The model

a. Model description

We use the so-called ATL6–26 experiment of the "CLIPPER" model based on the primitive equation code Océan Parallélisé (OPA8.1) developed at the Laboratoire d'Oceanographie Dynamique et de Climatologie (LODYC; Madec et al. 1998). It is a second-order finite-difference model with a rigid lid and z coordinates in the vertical direction. The horizontal grid is a Mercator isotropic grid with resolution ⅙° at the

equator, covering the Atlantic Ocean from Drake Passage to 30°E and from Antarctica (75°S) to 70°N. Vertically, the model has 42 geopotential levels spaced from 12 m near the surface to 200 m below 1500 m. We refer the reader to Treguier et al. (2003) for a description of a previous experiment with this model and only mention here some changes in the mixing characteristics that were made for this study.

A horizontal biharmonic operator is used for lateral mixing of momentum with a coefficient of 5.5×10^{10} m^4 s^{-1} at the equator, varying with the third power of the grid spacing. Mixing of temperature and salinity is Laplacian and isopycnal with a coefficient of 150 m^2 s^{-1} at the equator, also varying in latitude with the grid spacing. The vertical mixing of momentum and tracers is calculated using a second-order closure model (Madec et al. 1998). In case of static instability, the vertical mixing coefficients are set to the large value 1 m^2 s^{-1}.

With a view to this EUC study, an additional mixing parameterization was superimposed in the equatorial region after a series of tests (Michel and Treguier 2002). Having noted that the original CLIPPER experiment produced a too-intense EUC in the Gulf of Guinea, an enhanced Laplacian mixing of momentum added in the upper equatorial band was found to satisfactorily correct this flaw. This additional mixing term may be justified by the absence of inertial instability in the original model, for lack of a spatial resolution appropriate to this process. The added Laplacian diffusion of momentum has a constant coefficient 10^3 m^2 s^{-1} between 1°N and 1°S and above 60 m, decaying to zero at 3° of latitude and 120-m depth.

The model is initialized with the climatology of Reynaud et al. (1998) and integrated from rest starting in 1990, using a daily forcing. The upper tropical ocean is spun up after three years by 1993, and the midlatitude upper-ocean circulation is globally adjusted after 1995 (the deep ocean requires much longer time to equilibrate). The results presented below were obtained using winds from the European Centre for Medium-Range Weather Forecasts (ECMWF) 15-yr Reanalysis (ERA-15) for years 1990–93 and the analysis afterward up to year 2002. Our study of the EUC uses the 10-yr period 1993–2002. As Bryan et al. (1995) showed that simulations of the tropical Atlantic circulation may be sensitive to the wind stress forcing product, another experiment was performed using weekly European Remote Sensing Satellite (ERS) winds from 1993 to 2000, and previously spun up for three years by averages of the same ERS winds. Although this simulation produced a slightly reduced EUC (the extrema of the ERS equatorial easterlies are weaker than the ECMWF ones), both experiments produced very similar results for what concerns time variability. The longer ECMWF time series led us to retain this forcing.

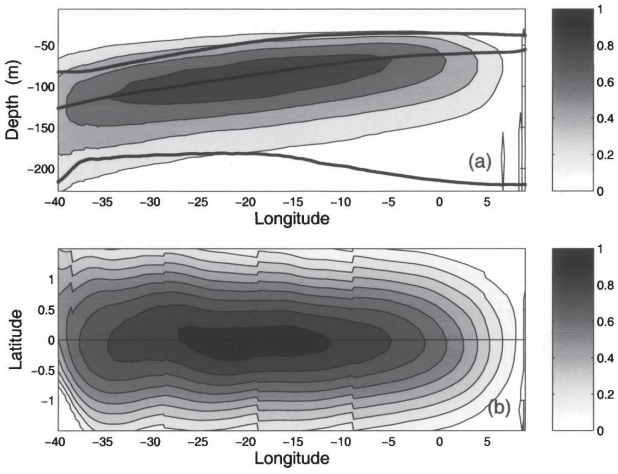

FIG. 1. Ten-year average (1993–2002) longitudinal distributions of the EUC velocity magnitude (m s^{-1}) in the CLIPPER simulation. (a) Vertical distribution at latitudes of maximum velocity. Contour interval is 0.2 m s^{-1}. Velocities are set to zero where the zonal component is negative. Superimposed are isopycnals σ_θ = 24.4, σ_θ = 25.5, and σ_θ = 26.65 kg m^{-3}, which approximately mark the upper limit, core, and lower limit of the EUC. (b) Lateral distribution at depths of maximum velocity at each longitude, contour interval 0.1 m s^{-1}. Jumps in the isotachs reflect the model vertical discretization.

b. The model time-averaged EUC

Figures 1 and 2 provide elements for a first evaluation of near-equatorial currents and properties in the model, based on 10-yr averages of the variables. The vertical and lateral velocity distributions (Fig. 1) exhibit the well-known jetlike structure of the EUC, located on average between 50- and 250-m depth and within ±1.5° of latitude. Along the equator we observe an acceleration region west of ~25°W, nearly constant velocities between 25° and 15°W, and a gradual decrease to the African coast. This longitudinal velocity pattern is qualitatively similar to the one described by Wacongne (1989) using the model of Philander and Pacanowski (1986a), yet shifted eastward by 5°–10° of longitude, and more representative of the real EUC termination in the Gulf of Guinea. The EUC core has properties ($T \sim 20$°C, $\sigma_\theta \sim 25.5$ kg m^{-3}) comparable to those in the real ocean, but its density increases eastward at a lower rate than observed by Gouriou and Reverdin (1992) from the FOCAL data (from 25.5 to 25.6 kg m^{-3} between 35° and 4°W, instead of from 25.3 to 25.7 kg m^{-3}). Comparison with the climatology is more satisfactory for the vertical temperature distribution (Figs. 2a,b) than for the salinity one (Figs. 2c,d), par-

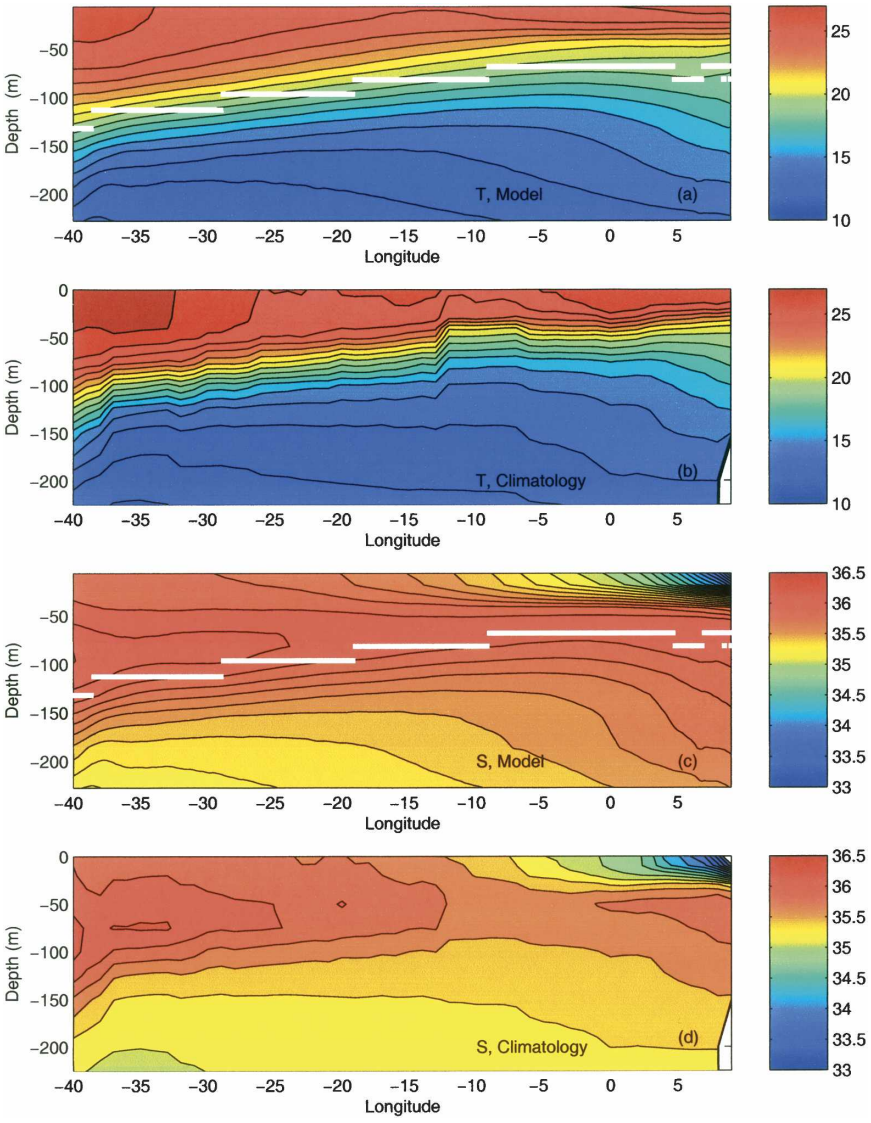

FIG. 2. Ten-year average (1993–2002) vertical distributions of (a) model temperatures (°C) and (c) salinity along the equator with the depths of the EUC averaged maximum velocities superimposed. Equatorial vertical distributions of (b) temperature and (d) salinity from the climatology of Reynaud et al. (1998). Contour intervals are 1°C for temperature and 0.1 psu for salinity.

ticularly in the eastern half of the basin where salinities are too high in the model. This problem, which makes the lower part of the EUC too dense in the Gulf of Guinea, was found to be caused by the inaccuracy of the centered advection scheme in the presence of sharp vertical gradients. It has no consequence on the results presented in this study, which mainly concern the western and central ocean. A 2.7-yr averaged zonal velocity profile at 0°, 28°W presented by Weisberg et al. (1987) provides a more quantitative element for comparison (Fig. 3a). The model counterpart, interpolated onto the current-meter sampling depths (Fig. 3b), exhibits a similar averaged EUC thickness (150 m based on a $U > 0.2$ m s^{-1} criterion, as compared with 160 m from the data), but slightly higher velocities at the undercurrent maximum (0.9 m s^{-1} as compared with 0.8 m s^{-1}).

Seasonally, the model reproduced the well-documented vertical excursions of the EUC core (Weisberg et al. 1987), which are most pronounced in the western basin (e.g., at 35°W from a depth of 85 m in May to 130 m in September). The model also predicts significant variations of the longitudinal distribution of the EUC core velocities (Fig. 4). West of 35°W, these are highest (up to 1 m s^{-1}) during the winter and spring, whereas in

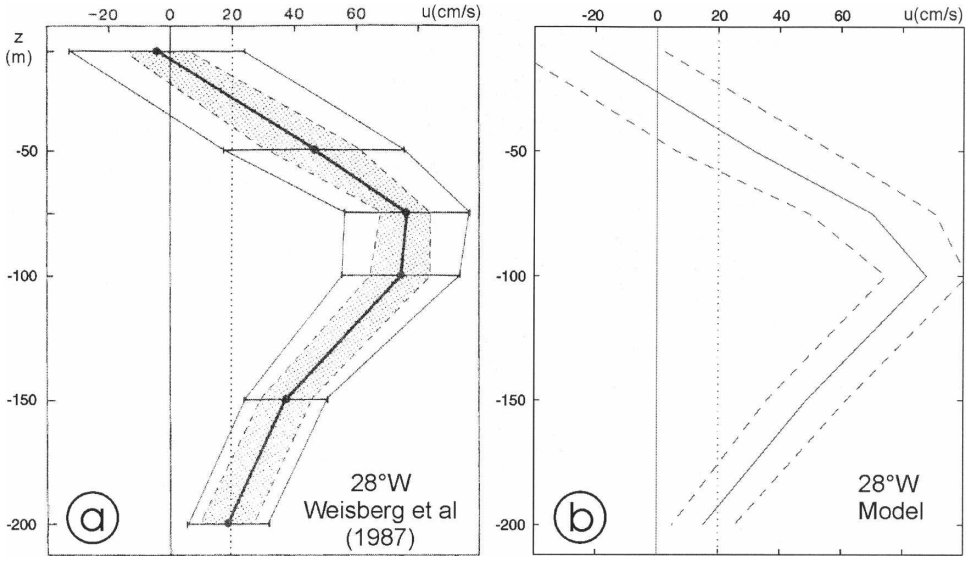

FIG. 3. (a) Zonal velocity profile (with root-mean-square deviations and 90% confidence interval) from 2.7-yr-long measurements at 0°–28°W (reproduced from Weisberg et al. 1987). (b) Ten-year (1993–2002) average zonal velocity profile at 0°, 28°W from the CLIPPER simulation, interpolated onto the measurement levels. The 20 cm s^{-1} velocity threshold used to estimate the EUC transport is shown in both panels.

the central part of the basin they reach a maximum (up to 1.2 m s^{-1}) during the second half of the year. The longitudinal plateau of the core velocity mentioned above is most pronounced and extends farther west during the first period. Real EUC velocity maxima obtained from a set of shipborne ADCP sections across the undercurrent (Table 1), though only providing a sparse longitudinal sampling, suggest an overall satis-

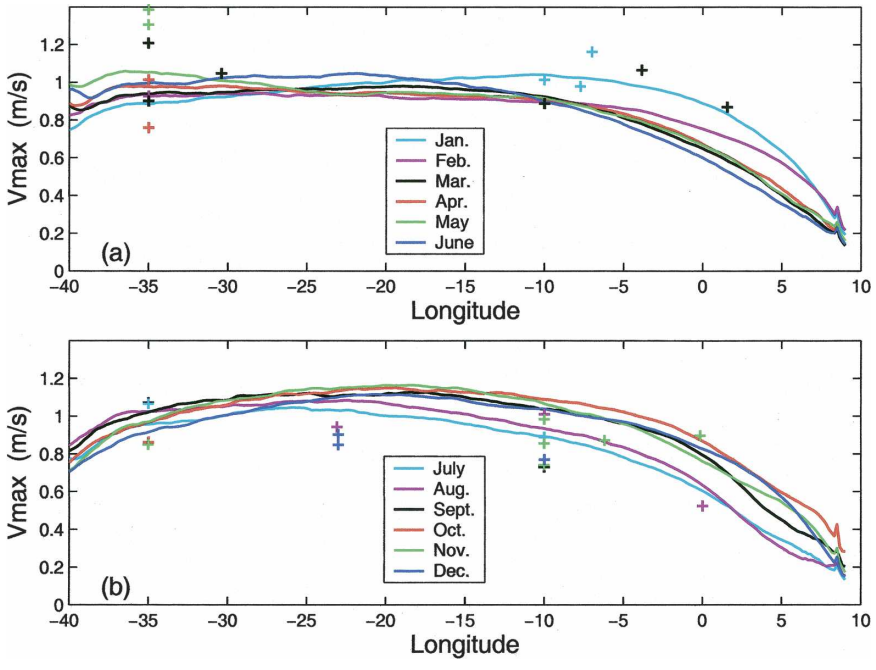

FIG. 4. Ten-year average (1993–2002) monthly longitudinal distributions of the EUC maximum velocities in the model. The shipborne ADCP values reported in Table 1 are superimposed.

TABLE 1. Estimates of EUC maximum velocity, depth of maximum velocity, and transport from shipborne ADCP measurements during cross-equatorial sections. The transports were estimated using velocity values within the 0.2 m s^{-1} isotach. Cases with no transport estimate correspond to an incomplete sampling of this domain.

Longitude (°W)	Month	Year	V_{max} (m s^{-1})	Z_{Vmax} (m)	T (Sv)	Cruise
−35	10	1990	0.86	−120	23	Meteor-142
−35	5	1991	1.38	−40	33	Meteor-163
−35	11	1992	0.85	−125	15.5	Meteor-222
−35	2	1993	0.93	−108	22	CITHER-1
−35	3	1994	0.90	−72	18	Meteor-273
−35	9	1995	1.04	−96	31.5	ETAMBOT-1
−35	4	1996	1.01	−56	23.5	ETAMBOT-2
−35	7	1999	0.95	−94	17.5	EQUALANT-99
−35	4	2000	0.76	−57	19	Meteor-471
−35	3	2001	1.21	−79	21	Ron-B
−35	5	2002	1.30	−38	13.5	Meteor-532
−30.4	3	1994	1.05	−58	20.5	CITHER-2
−23.1	8	1999	0.91	−96	13.5	EQUALANT-99
−23	12	2001	0.85	−77		PIRATA-10
−23	12	2002	0.90	−81		PIRATA-11
−10	9	1997	0.62	−81	8.8	PIRATA-1
−10	1	1998	0.95	−57	11.5	PIRATA-3B
−10	8	1999	1.01	−60	23	EQUALANT-99
−10	3	2000	0.89	−48	6.7	PIRATA-6
−10	7	2000	0.75	−64	11	EQUALANT-00
−10	11	2000	0.80	−59	6.6	PIRATA-8
−10	11	2001	0.72	−75	5.7	PIRATA-9
−10	12	2001	0.77	−71		PIRATA-10
−10	11	2002	0.98	−65	10.5	PIRATA-11
−7	1	1995	1.16	−60	17.5	CITHER-3
−7.7	1	1998	0.98	−57		PIRATA-3A
−6	11	1998	0.87	−65		PIRATA-2A
−3.8	3	1993	1.06	−60	13	CITHER-1
0.0	8	2000	0.52	−44	2.8	EQUATANT-00
−0.1	11	1998	0.90	−65		PIRATA-2B
1.5	3	1995	0.87	−60	6.9	CITHER-3

factory model behavior (Fig. 4). However, these instantaneous in situ estimates are influenced by intraseasonal (e.g., Düing et al. 1975) and pluriannual EUC variations (Weisberg et al. 1987), which make a more detailed comparison difficult.

That the model reproduces these higher and lower frequency variations is illustrated in Fig. 5, which shows the time–longitude distributions of the EUC maximum velocity and transport from the 5-day model outputs. The high and low frequencies significantly blur the annual signal and, if a correct representation of reality, they indeed illustrate that 2–3-yr-long time series at a single longitude may not suffice to reveal an annual cycle. On the other hand, seasonal patterns do show up in the 10-yr model time series. These are, for the EUC velocity, an autumn maximum most pronounced in the central part of the basin, and for the transport, a similar maximum complemented by another one during spring in the western basin. The spring feature is less discernible in the velocity diagram, yet is also present in some years. The recurrence of these extrema, if not their quantitative repeatability, justifies constructing a model EUC annual cycle from the 10-yr monthly averages of the undercurrent velocity maxima and transports.

3. The annual cycle of the model EUC

a. Description of the annual cycle

The 5-day EUC model transports were computed over the domain within the 0.2 m s^{-1}eastward velocity isotach. Defining the undercurrent cross section from the velocity modulus led to seasonal transports differing by less than 2 Sv from those presented here. The computation was furthermore limited downward to 250 m and upward to 24 m in order to suppress a possible near-surface contribution during shoaling periods of the EUC. Such periods, during which the eastward flow even surfaces at times, have been often observed in the western basin (e.g., Bourlès et al. 1999) and are reproduced by the model. We here chose to limit the undercurrent upward to 24-m depth, but trials using 0 and 48 m only led to minor changes in the seasonal transport

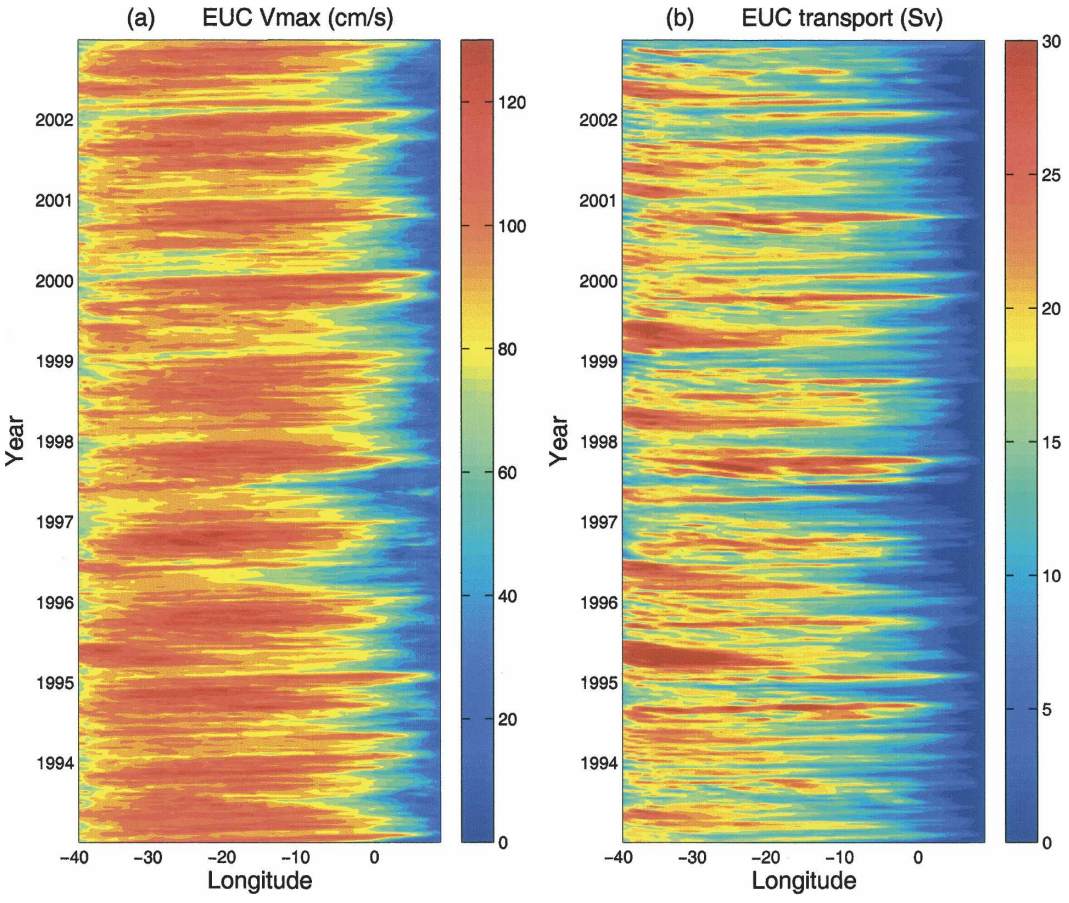

FIG. 5. Pluriannual longitude–time diagrams of the (a) model EUC maximum velocity and (b) EUC transport within the 20 cm s^{-1} isotach.

patterns and extrema (<2 Sv). The annual cycles of the EUC transport, maximum velocity, and cross section are displayed in Fig. 6.

The transport (Fig. 6a) exhibits the two maxima mentioned in the introduction, namely, an "autumn" one (August–November) in the basin interior and a "spring" one (January–June), most pronounced at 40°–35°W near the western boundary but extending eastward to about 10°W. Examination of the annual cycles of the undercurrent velocity maximum (Fig. 6b) and cross section (Fig. 6c) shows that, while the model autumn transport maximum is the combined result of maxima in the two parameters, the spring extremum is mostly contributed to by an increase of the cross section.

Figure 7 further decomposes the cross-sectional variations into those of the EUC thickness and width. Both parameters contribute to the autumn increase of the cross section, though at a 2-month time interval. The EUC thickness is highest at 10°–15°W in August (Fig. 7a), mostly because of a deepening of the undercurrent lower limit, which reaches down to about 250 m. At the same longitudes, the EUC width (Fig. 7d) exceeds 400 km in October, a consequence of poleward displacements of its northern and southern boundaries. Examining the monthly horizontal flow patterns (not shown), this broadening of the undercurrent seems to be caused by a lateral supply from both hemispheres in the August–November period, a likely enhancement of convergence at the depth of the undercurrent in response to the increased near-surface equatorial divergence.

The thickness effect is weaker on the spring transport maximum and even vanishes at 35°W where the May uplifts of the upper and lower EUC limits compensate each other in the model (Figs. 7a–c). Width variations are more important (Fig. 7d) and should be totally ascribed to motions of the northern limit of the undercurrent (Fig. 7f), as the southern limit is held fixed by the adjacent (and opposite) North Brazil Current (NBC). The winter–spring poleward displacement of the EUC northern boundary corresponds to a period when the current is mostly fed in its westernmost part

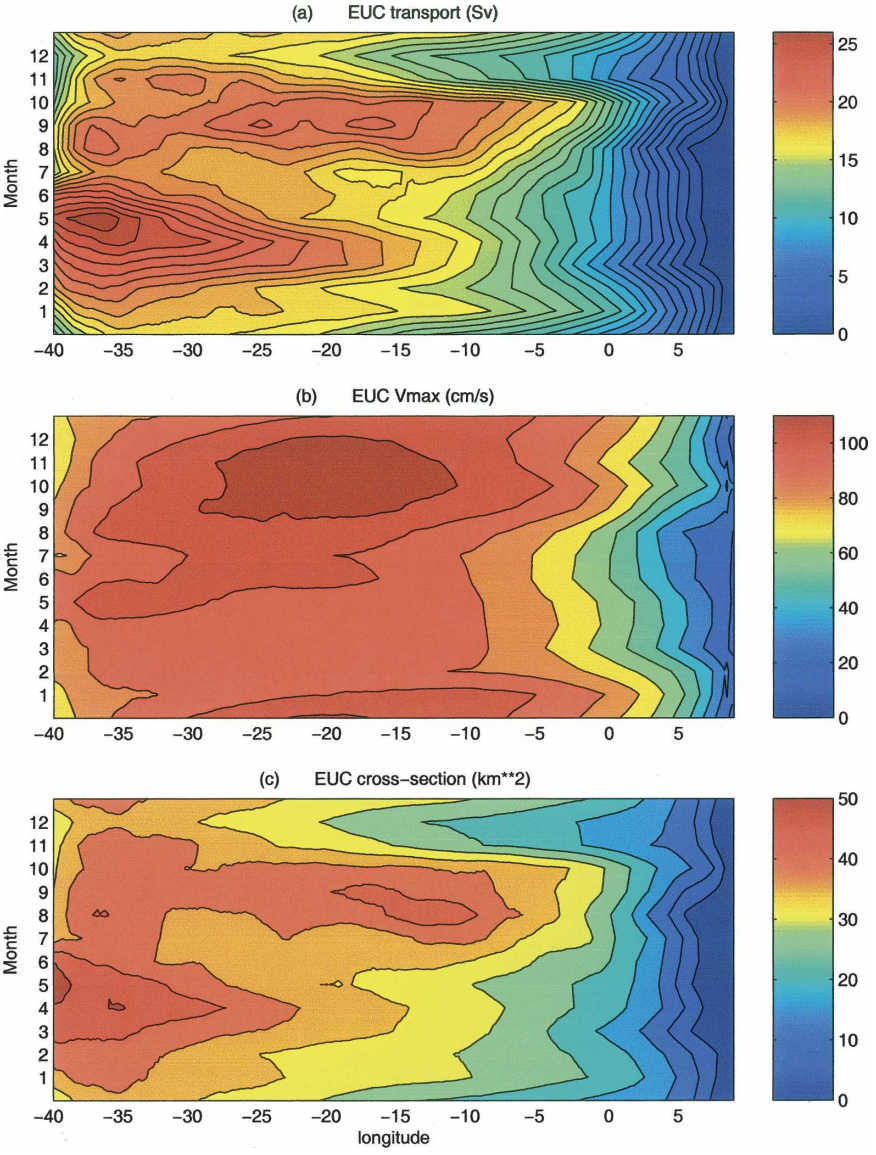

FIG. 6. Annual cycles of the (a) model EUC transport within the 20 cm s^{-1} isotach (contour interval 1 Sv), (b) EUC maximum velocity (contour interval 10 cm s^{-1}), and (c) EUC cross section (contour interval 5 km^2), estimated from the 1993–2002 model outputs.

from an anticyclonic loop of the NBC (Schott and Böning 1991). The current boundary moves equatorward again from May onward when the NBC loop extends farther northwestward along the coast and starts supplying the NECC instead of the EUC.

The above basinwide description generally matches the simulated double-maximum EUC cycles presented for individual longitudes in previous studies. Philander and Pacanowski (1986b; their Fig. 3) find both maxima at 30°W, but only the autumn one at 10°W. This, as well as the similar result of Hazeleger et al. (2003, their Fig. 2) at 35° and 20°W, fits in with the longitudinal shift of the two features in Fig. 6a. Schott and Böning (1991, their Fig. 8) also present a simulated double-maximum cycle at 35°W.

b. *The autumn maximum*

Prior to focusing on the spring transport intensification in sections 4 to 6, we first briefly comment on the autumn maximum as seen in the CLIPPER simulation. Though generally recognized, this feature appears with variable conspicuousness in the few observed transport cycles that were published. A reason for this might be its longitudinal dependence suggested by Fig. 6a. It is

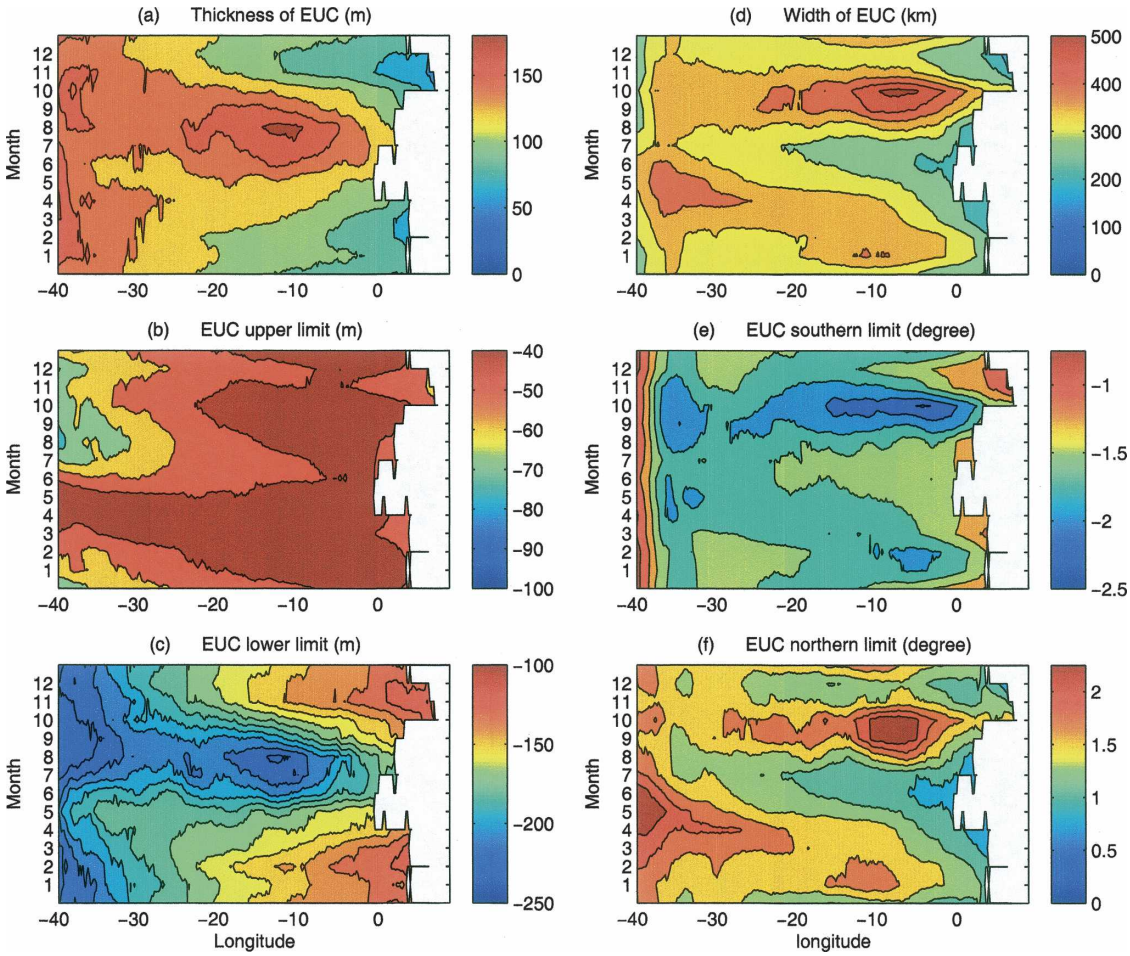

FIG. 7. Annual cycles of (a) model EUC thickness; (b), (c) EUC upper and lower limits; (d) EUC width; and (e), (f) EUC southern and northern limits.

weakly developed, though present, in the annual cycle built from 25°–33°W data by Katz et al. (1981) and shows up more clearly at 23°W in the FOCAL data analyzed by Hisard and Hénin (1987), as in recent 1-yr (2002) current-meter time series (Provost et al. 2004). Although Weisberg et al. (1987) do not mention the autumn maximum in their analysis of a SEQUAL time series at 28°W, local maxima exist in their three samplings of an August-to-October period.

The autumn transport maximum was often related (and ascribed) to the intensification of easterly winds and zonal pressure gradient in the same season (e.g., Hisard and Hénin 1987). This interpretation rests on studies of Philander and Pacanowski (1980) and Katz and Garzoli (1982), who showed that it does not take more than about a month after the onset of westward winds for the undercurrent to develop. Philander and Pacanowski (1986a) further emphasized a near-equilibrium response of the tropical Atlantic to the seasonal wind cycle, a behavior that Philander and Chao (1991) related to the limited width of the equatorial Atlantic. Figures 8a and 8b show the seasonal cycles of the equatorial ECMWF zonal wind stress and 23°–10°W dynamic height differences in the model, which illustrates the above relations. The model levels retained for the dynamic height computations (55 m/452 m) are close to those used in previous data analyses by Katz et al. (1977) and Lass et al. (1983) (50 m/500 m). Although equatorial velocities at 500-m depth have seasonal variations of order 10 cm s^{-1} (Schott et al. 2003), the two former studies show that dynamic heights computed with this reference level can explain the autumn EUC maximum. This also holds in the model, with a 23°–10°W pressure difference largest in August–September at the period of the autumn transport maximum and 1–2 months after the maximum of local zonal wind stress. In the same figure, however, the 35°–23°W pressure difference in the region of the spring maximum

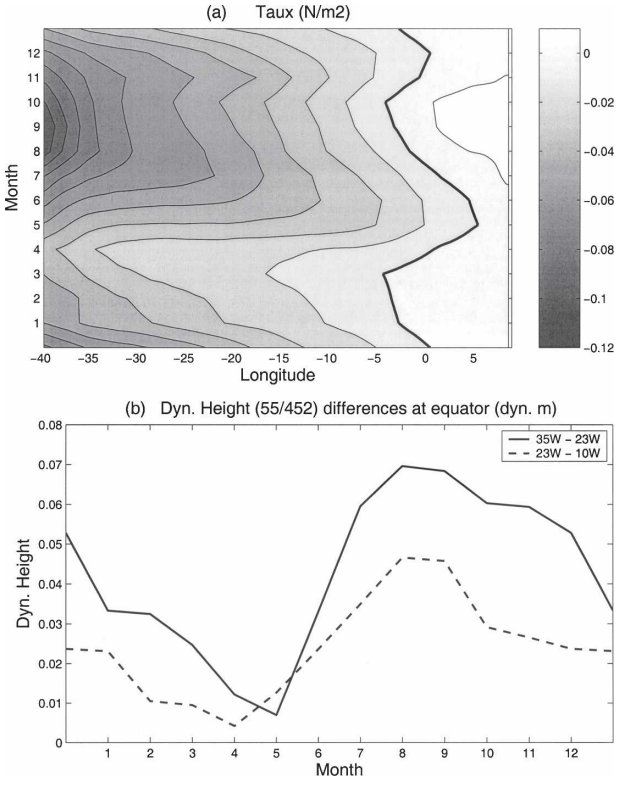

FIG. 8. (a) Annual cycle of the ECMWF zonal wind stress component along the equator. Contour interval is 0.01 N m^{-2}, and the thick line shows the zero contour. (b) Annual cycles of the model dynamic height (55 m/452 m) differences 35°W minus 23°W and 23°W minus 10°W along the equator.

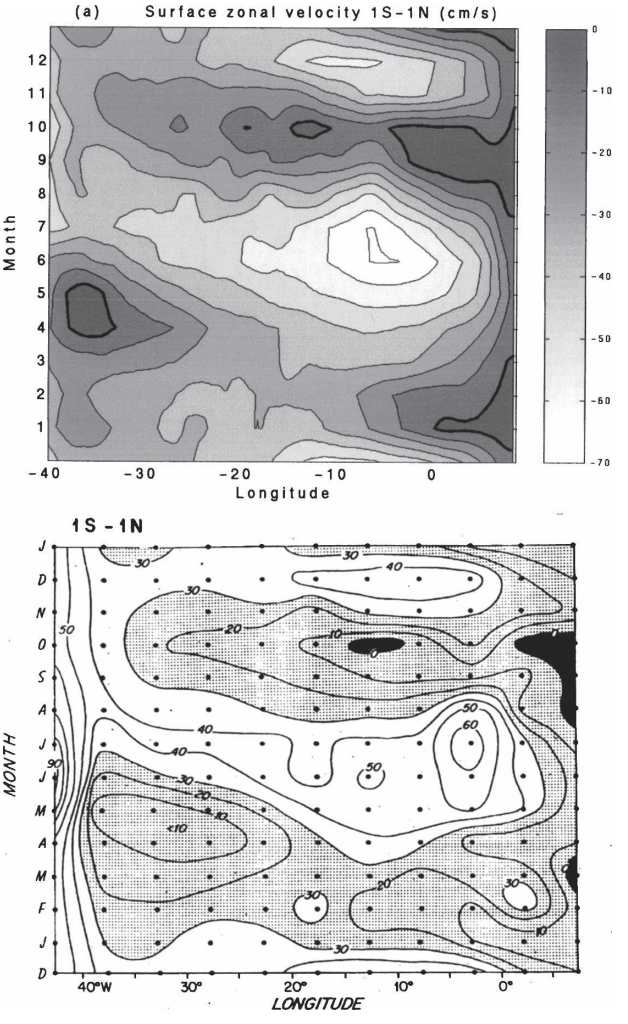

FIG. 9. (a) Annual cycle of the model surface zonal velocity averaged over the 1°S–1°N latitude band (contour interval 10 cm^{-1}). (b) Annual cycle of surface velocity (cm s^{-1}) averaged over 1°S–1°N, estimated from ship drift data (positive velocities are westward) (from Richardson and McKee 1984).

shows a similar annual cycle with, in particular, a nearly vanishing gradient in May when the EUC transport is highest. The rationalization of the spring maximum must obviously be different from that of the autumn maximum.

4. Signs of a spring EUC transport intensification in the observations

a. Indirect manifestation in surface equatorial currents

Several authors (Philander 1973; Katz and Garzoli 1982) have observed that the EUC transport variations generally mirror those of the equatorial surface zonal current. Considering the difficulty in measuring the undercurrent, evaluating the related model surface flow against its more easily measured real counterpart may therefore help to check the presence of a double EUC maximum in the ocean. The seasonal cycle of the model zonal surface velocity along the equator (Fig. 9a), indeed, also exhibits two maxima: one in April–May near the western boundary and the other one in October in the central part of the basin. Disregarding the extensions of these features to the African coast, which are associated with the average eastward shoaling of the undercurrent, this pattern is a close reflection of the undercurrent seasonal cycle (Fig. 6a). Still neglecting the easternmost quarter of the basin, an EUC surfacing (recognized by eastward surface velocities) is observed at 35°–38°W in April–May during the transport maximum, and a more limited one around 12°W in October. Although the spring feature is a clear surface imprint of the undercurrent transport maximum, it should not be regarded as causing the latter for, as noted above, the transport high survives a withdrawal of the near-surface velocities, and no increase of the undercurrent thickness accompanies it in the model.

The comparison of the model equatorial surface flows with those of the real ocean [Fig. 9b, reproduced from Richardson and McKee (1984)] reveals similar patterns. It shows, in particular, that the model April–May surface imprint of the undercurrent maximum has a quantitatively comparable counterpart in the real ocean, though with no surfacing in these data.

b. *Indirect indication from western boundary current transports*

The closeness of the spring EUC transport maximum to the western boundary suggests that it might be related to variations in the western boundary currents. Analyses based on hydrography (Metcalf and Stalcup 1967) and current measurements (Schott et al. 1998) showed that the EUC is fed by a partial eastward retroflection of the North Brazil Current between 0° and 4°N. Two current-meter arrays deployed across the NBC, one at the equator upstream of the current bifurcation (Schott et al. 1998) and the other one near 4°N just downstream of it (Johns et al. 1998), provide elements of comparison with the EUC variations. Upstream of the bifurcation Schott et al. (1998) observed a mean NBC transport of ~22 Sv above 300-m depth, with seasonal variations not exceeding ±2.5 Sv. Comparing this with the results of Johns et al. (1998) at 4°N, the same authors noted "an astonishing amplification of the seasonal transport cycle" between the two latitudes. The 4°N measurements indeed show a 0–300-m NBC transport varying from a minimum of 10 Sv in April–May to a maximum of 31 Sv in August. Although the reported transports were estimated over a vertical range exceeding that of the EUC, the pronounced April–May minimum of the boundary current downstream of the EUC branching, exactly coincident with the spring maximum of the undercurrent in the model, is another indication that the latter might be real.

c. *Direct current measurements*

Several studies have reported high values of the undercurrent transport during spring when the easterly trades are minimum (Philander 1973; Katz et al. 1981; Hisard and Hénin 1987; Schott et al. 1998; Bourlès et al. 1999). Because of the snapshot character of most measurements, however, the composite annual cycles that can be produced are not unquestionable. We noted above that the spring EUC transport maximum in Katz et al. (1981) mostly rested on an isolated estimate. Similarly, although the shipborne ADCP transport values at 35°W in Table 1 show maxima in May (33 Sv) and September (31.5 Sv), the range of all other estimates (from 13.5 to 23.5 Sv) prevents one from drawing any firm conclusion about a double-maximum cycle. The few available time series of EUC velocities (Weisberg et al. 1987; Provost et al. 2004) show spring intensifications during certain years, but they are not long enough to produce undoubted annual cycles, given the interannual variability. Variations of equatorial velocities might also not be a good indication of transport variations, as the model suggests that the EUC cross-section area also varies.

The equatorial velocity time series of Weisberg et al. (1987) at 0°, 28°W sampled three spring seasons. Although no recurring spring intensification is visible in their series of zonal velocities (values exceeding 1 m s^{-1} only appear in two of the three seasons), a vertical mode analysis performed by those authors using time domain empirical orthogonal functions suggests that a significant part of the EUC energy is to be ascribed to this season. Owing to the different vertical positions of the EUC in spring (shallower) and autumn (deeper), the spring configuration is recognized in the first vertical mode of the decomposition, which accounts for 53% of the total variance of the observed zonal velocity. The same EOF decomposition on the model zonal velocity at 0°, 28°W produced a first vertical mode profile very similar to that of Weisberg et al. (1987, their Fig. 7) also associated with a recurring spring extremum. The contribution of this first mode to the variance was found to be 41%, that is, lower than in the real ocean. Since the model does exhibit the EUC spring maximum, this comparison, although done on the velocities (not the transports), might be another indication that the spring intensification is real.

5. Possible causes of the spring EUC maximum

a. *Space–time variations of the equatorial zonal wind stress*

Variations of the zonal wind stress and associated pressure gradient force along the equator have long been regarded as the primary driving agent of the EUC. Using data to the west of 10°W from the GATE and EQUALANT experiments (in 1974 and 1963, respectively), Katz et al. (1977) estimated a zonal pressure gradient varying from nearly vanishing values in winter and spring to a maximum in late summer and autumn. After a high spring value of the undercurrent transport had been observed during the Global Weather Experiment of 1978–80 (Katz et al. 1981), Katz and Garzoli (1982) suggested that this maximum might be caused by a temporarily unbalanced gradient pressure force after the cessation of the wind in early winter.

Lass et al. (1983) proposed a different interpretation of the spring maximum: They observed that the ITCZ

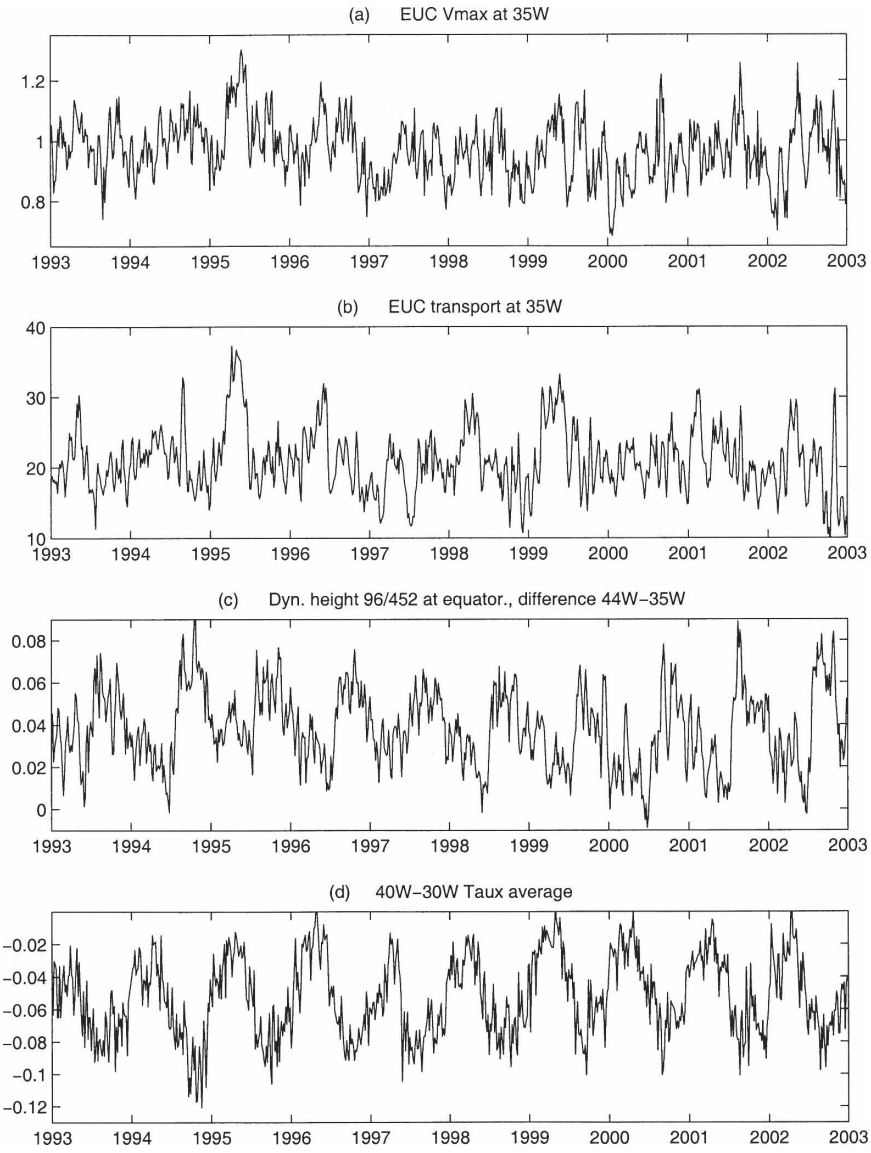

FIG. 10. Time series (1993–2002) of the following model and forcing parameters: (a) EUC maximum velocity (m s^{-1}) at 35°W; (b) EUC transport (Sv) at 35°W; (c) difference of dynamic height 96 m/452 m (dyn m) between 44° and 35°W along the equator; and (d) zonal wind stress (N m^{-2}) averaged between 40° and 30°W along the equator. Note that dynamic heights are computed at 96 m in (c) (we used 55 m in Fig. 8) to account for the westward deepening of the EUC.

winter position, which is usually around 2°N in the western Atlantic, may not reach such low latitudes in certain years. They suggested that, when this happens, it results in the maintenance of significant equatorial easterlies and zonal pressure force during this period, which could cause high spring values. The maintenance of an eastward pressure force in the western part of the ocean was also regarded by Philander and Chao (1991) as the cause of a spring EUC maximum at 140°W in the Pacific Ocean, observed by Halpern and Weisberg (1989). Philander and Chao, however, remarked that, because of a lower zonal extent and reduced wind phase differences in the Atlantic, the maximum EUC speed should coincide with that of the easterly winds in this ocean.

To possibly detect such effects in the 10-yr CLIPPER simulation, we show in Figs. 10a–d the model variations of the EUC speed and transport at 35°W, those of the dynamic height difference at 44°–35°W in the EUC core, and the zonal wind stress averaged over the 30°–

40°W interval. Contrasting with the repeated annual cycles of the dynamic height and zonal wind component (Figs. 10c,d), the EUC variables (Figs. 10a,b) show more irregular time variations. High winter/spring transport values nevertheless stand out in Fig. 10b, themselves highly variable, from ~35 Sv in 1995 to no maximum in 2000. With reference to the suggestion of Katz and Garzoli (1982) that a temporarily unbalanced pressure force after the wind cessation might cause the spring intensification, we examine the case of April/May 1995 when both the EUC velocity and transport show well-defined maxima. There was, indeed, a sudden relaxation of the easterlies in December 1994, but this event preceded the model transport maximum by about four months, a long time lag if compared with the O(1 month) adjustment time found by Philander and Pacanowski (1980). The dynamic height difference between 40° and 30°W (not shown) was found comparable to that of other years when the maximum is lower, and the 1995 zonal wind minimum coincident with the EUC maximum was also not particularly pronounced. The 1995 model response, as those relative to other cases of pronounced EUC maxima (1996, 1999), therefore provide no particular support to the hypothesis of a temporarily unbalanced local pressure force after the wind cessation.

Following the idea of Lass et al. (1983) and Philander and Chao (1991) that the EUC variations at a given longitude might reflect those of the zonal pressure force to the west of this longitude, we now examine the time series of the dynamic height difference between 44° and 35°W (Fig. 10c). There exists, in 1995, a weak secondary maximum of dynamic height difference (>0.04 dyn m) coincident with the spring EUC maximum. However, an examination of the 44°–35°W wind stress average (not shown) did not reveal any concomitant signal. While this secondary pressure gradient maximum to the west of 35°W certainly contributes to the EUC event in the spring of 1995, it is therefore not a direct consequence of simultaneous zonal winds. Furthermore, other winter/spring periods of intense EUC in the model time series (1996, 1999) are not associated with pressure gradient signals. This does not plead in favor of a lagging wind effect over the westernmost part of the basin to generate the spring EUC maximum.

b. The rotational wind component

In his stationary boundary layer solution of the EUC, Pedlosky (1987) emphasized the undercurrent connections to nonequatorial flows, either through the western boundary layer or the ocean interior. Noting the difficulty to relate the spring intensification of the model EUC to a purely equatorial forcing, we now explore the possibility that nonequatorial winds might cause it. While Pedlosky's (1987) theory focused on the links between the subtropics and the equator, Liu and Philander (1995) stressed that the subtropical influence on the EUC, quite pronounced in terms of water properties, is hardly significant for what concerns the undercurrent speed. A nonequatorial contribution to the EUC variability should therefore be sought in the Tropics (equatorward of 10° latitude, say) rather than the subtropics. The tropical region is, indeed, one of strong seasonal variability induced by the meridional migrations of the intertropical convergence zone (ITCZ) from ~2°N in spring to ~10°N in autumn. Garzoli and Katz (1983) and Garzoli (1992), using observations and model simulations, found that the NECC has seasonal variations in phase with those of the wind stress curl. Johns et al. (1998) similarly found some correlation between the seasonal cycle of the North Brazil Current at 4°N and the interior wind stress curl. Here we look for a possible link between the EUC and the low-latitude wind stress curl.

In a study of the EUC of the Pacific Ocean, Kessler et al. (2003) showed that, despite the importance of nonlinearities at the equator, the wind curl forcing acting through linear Sverdrup dynamics contributes to the time-averaged zonal equatorial transports. They particularly pointed out configurations where northward gradients of the wind stress curl at the equator cause an eastward tendency of the EUC. In the Atlantic such a configuration exists in April (Fig. 11a) when the sharp meridional gradient of wind curl associated with the ITCZ occupies the domain 0°–2°N in the western basin. Because the ITCZ has moved northward by September, no such wind curl gradient is present near the equator during this month (Fig. 11b). Figures 11c and 11d display the familiar patterns of the Sverdrup function ψ obtained by integrating westward the ratio of the wind stress curl to the planetary vorticity gradient. Whereas in September the zonal Sverdrup transport along the equator is only significant (and westward) west of ~35°W, in April a pronounced eastward transport O(10 Sv) is associated with the equatorial wind curl gradient. Keeping in mind the stationary hypothesis inherent to the Sverdrup theory and the nonlinearities of equatorial dynamics, we observe, therefore, that the linear effect illustrated in Fig. 11c matches the EUC spring intensification and provides a potential explanation for it. We also note the extraequatorial character of the forcing suggested here, as the equatorial Sverdrup transport depends on the wind curl values on both sides of the equator through their westward-integrated difference.

In April, the prevailing positive values of ψ to the

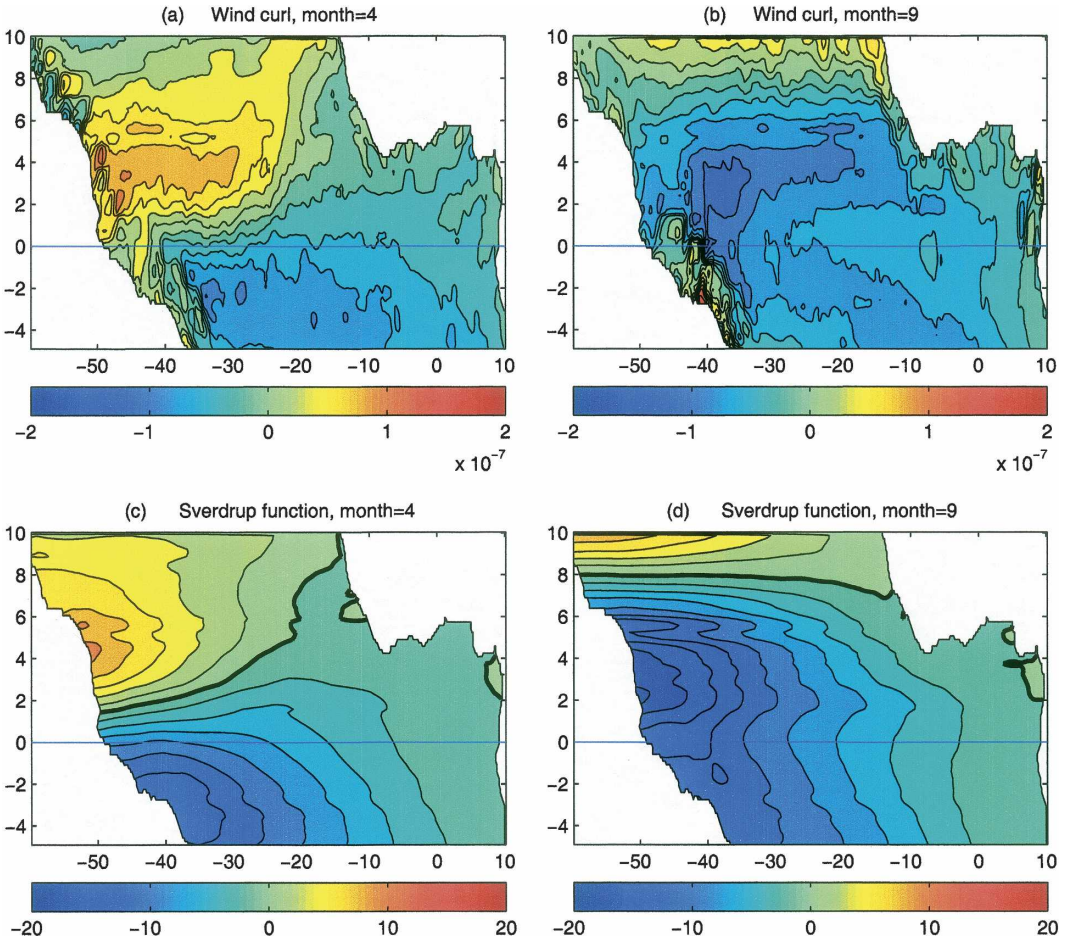

FIG. 11. (a), (b) Wind stress curl (10^{-7} N m^{-3}) and (c), (d) Sverdrup function (10^6 m^{3}s^{-1}) maps for the months of April and September, computed from the 10-yr (1993–2002) ECMWF wind time series used to force the model. Contour intervals are (a), (b) 2×10^{-8} N m^{-3} and (c), (d) 2×10^6 m^3 s^{-1}. The thick lines in (c) and (d) show the zero contours.

north of ~2°N reveal a cyclonic tropical gyre centered at 4°–6°N (Mayer and Weisberg 1993). Adjacent to the tropical gyre and to the south of it is the clockwise equatorial gyre, mostly located in the Southern Hemisphere in winter and early spring. The September situation is quite different, with the transition between the tropical and equatorial gyres shifted to about 8°N (Fig. 11d). The two western boundary flows inferred from the gyre patterns of Figs. 11c and 11d converge near 8°N in September to give the eastward NECC. In April their meridional convergence near the equator should similarly be at least partly balanced by an eastward flow that would temporarily reinforce the EUC. As another way to present this varying current pattern, we may regard the NECC as always present (with variable intensity) at the meridionally fluctuating boundary between the equatorial and tropical gyres. This current stands out by itself during the northward migration of the gyre boundary in summer and autumn but may occasionally merge with, and reinforce, the EUC when, during the winter and spring of certain years, the gyre boundary comes sufficiently close to the equator. Garzoli and Richardson (1989) observed this meandering of the NECC using an array of inverted echo-sounders at 28°W.

A particularity of the model EUC spring maximum, which fits in with the idea of a supply from the western boundary, is its intensification in the western part of the basin (Fig. 5b). The spring EUC maximum extends eastward to about 10°W (Fig. 6a). This is also consistent with the zonal variations of the 2°N–2°S zonal Sverdrup transport $\psi_{2N} - \psi_{2S}$ (Fig. 12), which exhibit an April maximum only to the west of 10°W, increasing westward to 40°W. In the same figure we observe that the rotational wind component has a counteracting effect on the EUC in summer, limited in the ocean interior

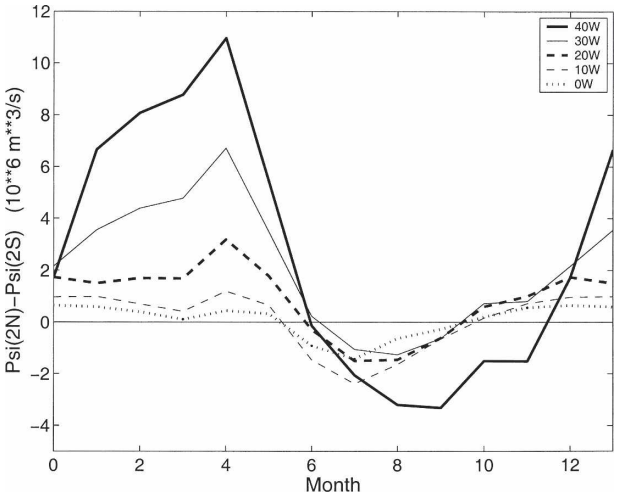

FIG. 12. Annual cycle of the variable $\psi_{2N}-\psi_{2S}$ at different longitudes showing the eastward decrease of the rotational wind forcing term.

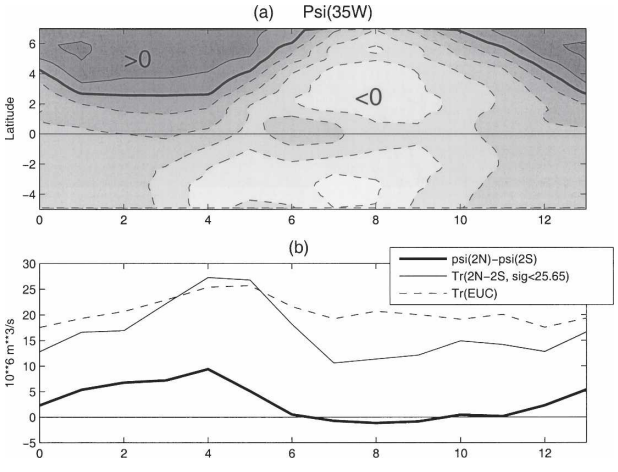

FIG. 13. (a) Annual cycle of the Sverdrup function (ψ) at 35°W, as a function of latitude. Contour interval is 3×10^6 m^3 s^{-1}, and the thick line shows the zero contour. (b) Annual cycle of Sverdrup transport ($\psi_{2N}-\psi_{2S}$) at 35°W. The model zonal transport at 35°W, between 2°N and 2°S and above σ_θ=26.65, and the model EUC transport are also shown.

(<2 Sv) but increasing and lasting over the autumn at 40°W. The western boundary supply of the EUC spring maximum contrasts with a contribution to the autumn maximum from the ocean interior. In section 3 we referred to monthly horizontal flow patterns at the EUC depth (not shown) exhibiting such a lateral supply from both hemispheres. Model transport computations across 2°N and 2°S between 35° and 10°W in the approximate density range of the undercurrent ($24.4 < \sigma_\theta < 26.65$) revealed equatorward transports in this period, up to ~5 Sv in August across 2°N and 2.5 Sv in September–October across 2°S.

c. *Time variations of Sverdrup function and equatorial Sverdrup transport at 35°W*

In this section we use the wind-deduced Sverdrup function ψ and equatorial Sverdrup transport $\psi_{2N}-\psi_{2S}$ as indices of the wind curl effect just described and examine whether their time variations at 35°W are related to those of the model EUC transport.

The 10-yr average annual cycle of the Sverdrup function at 35°W (Fig. 13a) illustrates the southward motion of the tropical/equatorial gyre boundary to near 2°N between February and April and the northward shift that is most pronounced in August. The time variations of $\psi_{2N}-\psi_{2S}$ at 35°W in Fig. 13b show that the wind curl effect is only active from December to May and vanishes during the remainder of the year. In the same figure, the 2°S–2°N model zonal transport between the surface and the base of the EUC, though higher than $\psi_{2N}-\psi_{2S}$ by about 10 Sv, exhibits similar variations with nearly constant values in summer and autumn and a high in April–May. The shift in magnitude between the two curves is probably due to equatorial intermediate and deep flows that, though less intense than the EUC, make a contribution to the vertically integrated transports (Schott et al. 2003). The time coincidence of the maxima in the two curves is good, with the decrease of the model 2°S–2°N transport in May–July only lagging that of the Sverdrup transport by about a month. A similar lag is visible on the model EUC transport curve also displayed in Fig. 13b. Considering previous observations of a rapid oceanic response to the wind stress curl at low latitudes (Garzoli and Katz 1983; Garzoli 1992), this quasi simultaneity of the peak values supports the idea that the spring intensification of the model transport is caused by the rotational wind effect.

To further evaluate this interpretation, Fig. 14a presents the pluriannual counterpart of Fig. 13a. In Fig. 14b are shown time series of $\psi_{2N}-\psi_{2S}$ and the EUC transport at 35°W, the latter with the mean value 21 Sv subtracted, and both represented by their monthly mean values. Lagged correlations between these two curves were found to culminate (at 0.68) when the EUC transport was shifted backward by two months. We then examined whether interannual variations of the wind curl parameters had counterparts in those of the EUC transport. The time variations of the line of zero wind stress curl (Fig. 14a) show that the yearly southernmost latitude of the equatorial/tropical gyre boundary fluctuates from less than 1°N to nearly 4°N. The years when the gyre boundary moves farther south in the simulation generally exhibit an intense EUC spring

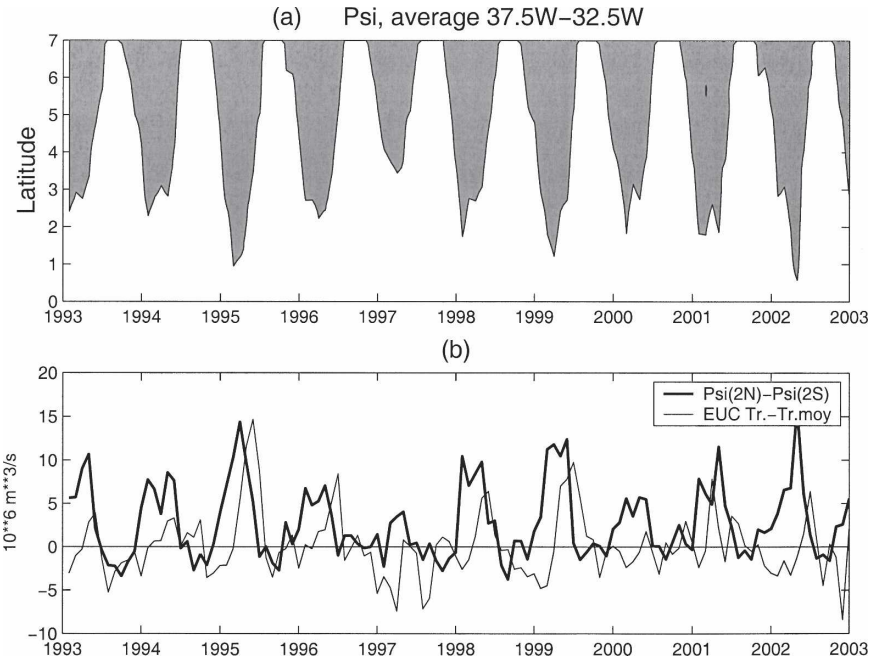

FIG. 14. (a) Ten-year latitudinal excursions of the zero isocontour of the Sverdrup function at 35°W. (b) Ten-year series of the variable $\psi_{2N}-\psi_{2S}$ at 35°W (thick line), and the model EUC transport variations about its mean value 21 Sv.

maximum (1995, 1999, but not particularly 2002). When the limit only reaches southward to 3°30′N in 1997, the EUC extremum can hardly be distinguished (Fig. 5b). Comparing the peaks of the equatorial Sverdrup transport to the EUC transport shows similar relations (Fig. 14b). The link between the two variables, however, is not obvious for some individual events, like the high spring Sverdrup transport of 2002. It is likely, therefore, that the effect of the rotational wind component on the EUC transport, though also supported by Fig. 14, is not exclusive during the winter/spring period. A remnant of equatorial zonal wind stress at the period of the southernmost ITCZ displacement might also contribute (Lass et al. 1983). A fraction of the EUC interannual variability might also just be internal variability explained by nonlinear ocean dynamics rather than by wind variations. In a model study of the NECC, Verdy and Jochum (2005) noted such variations not directly related to changes in the wind. To check the role of internal variability in the time variations of the EUC at 35°W, we carried out a 10-yr model run forced by the averaged wind seasonal cycle. The mean seasonal cycle of the EUC transport at 35°W for this run (not shown) was found similar to the one obtained from interannual forcing (dashed line in Fig. 13b) with, in particular, the spring maximum. The transport anomaly obtained by subtracting this mean seasonal cycle from the interannual variations (Fig. 15, dashed line) provides the internal variability. The absence of any spring intensification in this curve confirms the wind-forced character of the spring maximum well apparent in the anomalies from interannual forcing (Fig. 15, continuous line). The internal variability, however, is far from negligible, with a standard deviation of 1.35 Sv, as compared with 2.35 Sv for the run forced interannually. It is possible, there-

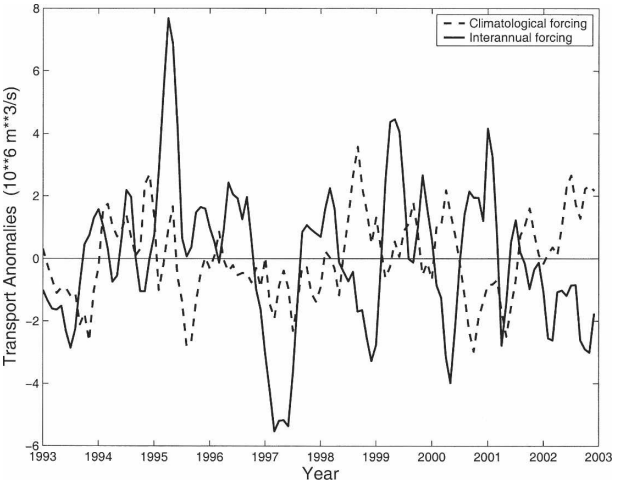

FIG. 15. Three-month filtered EUC transport anomalies at 35°W computed by subtracting the mean seasonal cycle to the transport. Continuous line: the model is forced by the 10-yr ECMWF wind series; dashed line: the model is forced by the mean seasonal wind cycle.

TABLE 2. Characteristics of the process experiments giving the EUC transports of Fig. 16.

	Wind	Basin geometry
SIM12	Spatially uniform sinusoidal annual cycle	Rectangular + flat bottom
SIM12C	Same as SIM12	Coast + topography
SIMRE	Realistic (*ERS-1*)	Coast + topography
SIMTAUX	*ERS-1*, $\tau^y=0$	Coast + topography

fore, that it might, on certain years, either enhance or counteract the wind-forced spring effect.

d. Process experiments

To further test the role of the wind stress curl on the EUC, we have used idealized experiments run by Thierry et al. (2004) with the same primitive equation model as CLIPPER. The Equatorial Undercurrent transport has been calculated in four experiments for the last model year, taking into account velocities greater than 0.2 m s^{-1} above 250 m (Table 2; Fig. 16). The first two experiments (SIM12 and SIM12C) are driven by spatially uniform zonal winds with a sinusoidal annual cycle. SIM12 has a rectangular basin and SIM12C has realistic coastline and topography. In both cases, the transport near 10°W is maximum in autumn, responding to the increase of the zonal wind stress along the equator (dashed lines, Fig. 16a). At 35°W (continuous lines), the annual cycle is weak and there is no trace of a spring maximum. When a realistic wind field is used (here in experiment SIMRE a climatology of wind stress from scatterometer measurements, years 1992–2000), a pronounced spring maximum appears in the EUC annual cycle at 35°W (Fig. 16b). Meridional variations of the *zonal* wind stress are the key element: the transport at 35°W still peaks in March–April in experiment SIMRETAUX, where the meridional wind stress has been set to zero (Fig. 16b). The idealized experiments of Thierry et al. (2004) therefore corroborate the inference drawn from the CLIPPER simulation that a wind stress curl is required to generate the spring maximum.

6. Discussion

a. Validity of Sverdrup dynamics

Our suggestion that the EUC spring maximum could be related to the nearly concomittant intensification of the equatorial Sverdrup transport should not be viewed as incompatible with the recognized importance of non-

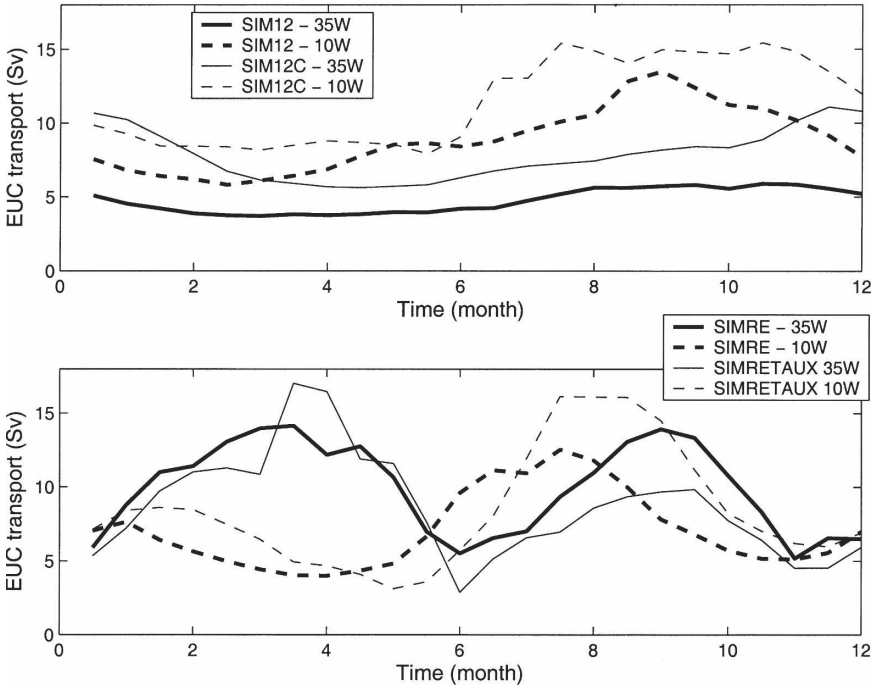

FIG. 16. Time series of EUC transport for one year in four idealized experiments run by V. Thierry (see Thierry et al. 2004, Table 1, for a complete description). (top) Two experiments with uniform zonal winds. Transports are averaged between 37.5° and 32.5°W (continuous lines) and 12.5°–7.5°W (dashed lines). (bottom) Two experiments with realistic wind stress.

linear dynamics at the equator and near the western boundary. Nonlinearities are generally thought to be important equatorward of about 2° of latitude (e.g., Pedlosky 1996). In a study of time-averaged and depth-integrated zonal equatorial transports in the Pacific Ocean, Kessler et al. (2003) estimated that taking into account the advective terms of the vorticity balance roughly doubles the transport over the Sverdrup solution. The linear forcing term nevertheless exists and, provided a rapid adjustment, must be enhanced in winter/spring when a strong meridional wind curl gradient occupies the equatorial band in the western basin. Kessler et al. showed how taking into account such gradients in the Pacific Ocean (using high-resolution wind products) greatly improves the realism of the EUC Sverdrup representation.

The spring EUC intensification takes place in the western part of the basin where nonlinearities are also particularly important (e.g., Verdy and Jochum 2005). Along the equator of the Pacific Ocean, however, Kessler et al. (2003) observed net counteracting effects of the advection and friction terms of the vertically integrated vorticity balance over the ocean width so that the difference of zonal transport from the Sverdrup transport was smaller near the western boundary than anywhere in midbasin. Although this applies to the Pacific, it suggests that along the equator deviations from the Sverdrup transport are not necessarily highest close to the western boundary.

Because of the expected contributions of the nonlinear terms to the zonal equatorial transport, we a priori regarded the variable $\psi_{2N}-\psi_{2S}$ more as a wind-deduced index of the suggested cause of the spring EUC maximum than as a transport value proper. It turned out, however, that $\psi_{2N}-\psi_{2S}$ had variations comparable in magnitude to those of the EUC or the 2°N–2°S model transports (Figs. 13 and 14). This might indicate a rapid decrease of nonlinearities away from the equator and a prevalence of Sverdrup dynamics at the two latitudes, 2°N and 2°S, in the simulated ocean interior. If so, and applying volume conservation in the domain bounded by 2°N and 2°S, 35°W and the African coast, $\psi_{2N}-\psi_{2S}$ should indeed provide an estimate of the model zonal transport across 35°W and between 2°N and 2°S. Another reason might be the dominance of the wind forcing term over the advective terms in the equatorial vorticity equation when, in spring, a strong meridional gradient of wind curl establishes along the equator.

b. Time-varying aspects

The above considerations hold for a stationary forcing. The suggested forcing of the EUC spring intensification, however, rests on the seasonal migration of the ITCZ between about 2° and 10°N. We quoted above previous observational results revealing some correlation between the seasonal variations of the NECC or the NBC and the wind stress curl of the interior ocean (Garzoli 1992; Johns et al. 1998). Several theoretical and model studies also emphasized that, owing to high speeds of the westward-traveling long Rossby waves in the Tropics, the Sverdrup circulation can adjust to the seasonal cycle of the wind stress at these latitudes. In the Atlantic, Döös (1999) showed that the seasonal variability (seen from satellite-deduced sea surface elevation) is highest equatorward of 5°N in the western basin and, to a large extent, can be explained by midlatitude Rossby wave theory. A seasonal cycle of the sea surface height just north of the equator and near the western boundary (3°N, 47°W; his Fig. 5) obtained from a numerical Rossby wave solution using the first three baroclinic modes indeed exhibits a minimum in March–April, as observed. Reflection of the Rossby waves at the western boundary near the equator can probably generate Kelvin waves that would propagate the seasonal signal eastward along the equatorial waveguide. As the pattern of sea surface height variability encroaches upon this equatorial band, it could also directly influence the equatorial variability through surface generated waves. While Brandt and Eden (2005) suggest that the annual cycle of the zonal velocity at 35°W and above 200 m might be explained in this way, Thierry et al. (2004) note the difficulty to separate the waves generated at the surface from those generated at the lateral boundaries in the surface layers of a nonlinear simulation. Whatever the origin, the expected equatorial propagation of zonal velocity signals causing the EUC spring maximum in the western basin must be fast (<1 month), either because of the high phase speed of Kelvin waves or because of local surface generation of Rossby waves.

7. Conclusions

The 10-yr CLIPPER simulation exhibits, on average, a well-defined annual cycle of the Atlantic EUC transport, characterized by two maxima. One develops in the interior of the basin in late summer and autumn when the equatorial easterlies are strongest, whereas the other is most pronounced near the western boundary in late winter and early spring when the easterlies relax. Despite their different longitudinal domains, the two maxima show no individualized signatures in the yearly averaged longitudinal distribution of the undercurrent transport.

While the autumn EUC maximum is generally recognized and is regarded as the oceanic response to the equatorial easterly wind stress, the spring high trans-

port values have been paid less attention. The more frequent references to velocity (rather than transport) variations in previous analyses of the EUC annual cycle may have been a reason for their relative neglect. This transport intensification, here studied from a particular CLIPPER experiment tuned on the yearly average undercurrent transport, was also present in the original simulation using different mixing algorithms near the equator. Changing the ECMWF wind forcing for the ERS one did not alter it. Several previously published model results exhibited the same double maximum at certain longitudes. The reality of the spring intensification, however, is still difficult to ascertain, given the limited number and generally short-lasting character of available current time series and the difficulty in measuring transport time series. We reported likely indirect manifestations of the EUC spring maximum but these, like the few velocity measurements, suggest rather than prove the existence of this maximum. Long current time series in the western part of the basin would be needed to confirm it and relate its occurrences and properties to the wind forcing parameters. We note that, in the Pacific Ocean, a well-defined EUC maximum also exists during the spring relaxation of the easterly trades (Philander et al. 1987; Halpern and Weisberg 1989).

Several studies have shown the rapid effects that variations of the interior wind stress curl at low latitudes have on the NECC and NBC. Although our diagnostic study suggests that the EUC similarly reacts to the low-latitude rotational wind stress component in spring, we have admittedly not explained the ensuing maximum nor its vertical structure, for the Sverdrup function gives, at best, information on the vertically integrated transport only. While at low latitudes the adjustment to Sverdrup dynamics results in a western boundary current (the NBC) and an intergyre jet (the NECC) that are surface intensified, the EUC equatorial spring maximum, though coincident with a shoaling of this current, remains a subsurface feature. This might indicate that the zonal wind forcing term, although weaker during this period, is still required to maintain a reduced westward surface South Equatorial Current above the EUC. A possible effect of the low-latitude rotational wind component on the EUC during spring reminds one of the inertial boundary layer solution derived by Pedlosky (1987) for a steady state in that it is also remotely forced. This regime clearly differs from that of the locally forced autumn maximum.

The rotational wind effect takes place when the boundary between the so-called equatorial and tropical gyres nears the equator. The role of the cyclonic tropical gyre in the ventilation of the equatorial thermocline has already been pointed out (Huang and Wang 2001; Inui et al. 2002), and the seasonality of the ventilation discussed (Lazar et al. 2002). Some results of these studies are found anew here, notably a dominant supply of the EUC through the western part of the ocean in spring and through the ocean interior in autumn. Those authors showed that the subtropical waters bound for the equator must skirt the region of positive wind stress curl that constitutes the tropical gyre. They noted that, in the Northern Hemisphere, the northern limit of this region may act as a barrier for these waters. When examining the EUC transport variations, it is the southern limit of the positive wind stress curl domain (i.e., the boundary with the equatorial gyre), and particularly its location relative to the equator, that is of importance.

The CLIPPER simulation suggests an intense interannual variability of the spring EUC transport with, in particular, a pronounced event in 1995. An unusual warming of the eastern equatorial region, associated with a blocking of upwelling along the African coast (the so-called Benguela Niños), was observed that very year (Gammelsrod et al. 1998). Philander (1986) noted that, in 1984 when a similar event occurred, the ITCZ (whose migrations match those of the zero wind stress curl line) moved southward farther than usual, a behavior that we have found to be also related to the high spring EUC transports. In a simulation of the tropical Pacific Ocean, Philander et al. (1987) observed a link between the spring EUC intensification and high sea surface temperatures in the eastern basin in April. In the Atlantic, a possible relation between the spring EUC transport in the western basin and the surface temperatures in the Gulf of Guinea might also deserve examination.

Acknowledgments. This study was supported by the Institut Français de Recherche pour l'Exploitation de la Mer (MA), the Centre National de la Recherche Scientifique (AMT), and the Institut pour la Recherche et le Développement (BB). We are indebted to Prof. F. Schott for providing the German shipborne ADCP data at 35°W and to R. Chuchla for computing the transport estimates of Table 1. We are also grateful to Dr. V. Thierry who shared the results of her numerical experiments and to Dr. R. Schopp for very useful discussions. The comments of two anonymous reviewers helped us to improve the manuscript.

REFERENCES

Bourlès, B., Y. Gouriou, and R. Chuchla, 1999: On the circulation in the upper layer of the western equatorial Atlantic. *J. Geophys. Res.,* **104,** 21 151–21 170.

Brandt, P., and C. Eden, 2005: Annual cycle and interannual variability of the mid-depth tropical Atlantic Ocean. *Deep-Sea Res. I,* **52,** 199–219.

Bryan, F. O., I. Wainer, and W. R. Holland, 1995: Sensitivity of the tropical Atlantic circulation to specification of wind stress climatology. *J. Geophys. Res.,* **100,** 24 729–24 744.

Döös, K., 1999: Influence of the Rossby waves on the seasonal cycle in the tropical Atlantic. *J. Geophys. Res.,* **104,** 29 591–29 598.

Düing, W., and Coauthors, 1975: Meanders and long waves in the equatorial Atlantic. *Nature,* **257,** 280–284.

du Penhoat, Y., and A. M. Treguier, 1985: The seasonal linear response of the tropical Atlantic Ocean. *J. Phys. Oceanogr.,* **15,** 316–329.

Gammelsrod, T., C. H. Bartholomae, D. C. Boyer, V. L. L. Filipe, and M. J. O'Toole, 1998: Intrusion of warm surface layers along the Angolan–Namibian coast in February–March 1995: The 1995 Benguela Niño. *South Afr. J. Mar. Sci.,* **19,** 41–56.

Garzoli, S. L., 1992: The Atlantic North Equatorial Countercurrent: Models and observations. *J. Geophys. Res.,* **97,** 17 931–17 946.

——, and E. J. Katz, 1983: The forced annual reversal of the Atlantic North Equatorial Countercurrent. *J. Phys. Oceanogr.,* **13,** 2082–2090.

——, and P. L. Richardson, 1989: Low-frequency meandering of the Atlantic North Equatorial Countercurrent. *J. Geophys. Res.,* **94,** 2079–2090.

Gouriou, Y., and G. Reverdin, 1992: Isopycnal and diapycnal circulation of the upper equatorial Atlantic Ocean in 1983–1984. *J. Geophys. Res.,* **97,** 3543–3572.

Halpern, D., and R. H. Weisberg, 1989: Upper ocean thermal and flow fields at 0°, 28°W (Atlantic) and 0°, 140°W (Pacific) during 1983–1985. *Deep-Sea Res.,* **36,** 407–418.

Hazeleger, W., P. de Vries, and Y. Friocourt, 2003: Sources of the equatorial undercurrent in the Atlantic in a high-resolution ocean model. *J. Phys. Oceanogr.,* **33,** 677–693.

Hisard, P., and C. Hénin, 1987: Response of the equatorial Atlantic Ocean to the 1983–1984 wind from the Programme Français Océan et Climat Dans l'Atlantique Equatorial cruise data set. *J. Geophys. Res.,* **92,** 3759–3768.

Huang, R. X., and Q. Wang, 2001: Interior communication from the subtropical to the tropical oceans. *J. Phys. Oceanogr.,* **31,** 3538–3550.

Inui, T., A. Lazar, P. Malanotte-Rizzoli, and A. Busalacchi, 2002: Wind stress effects on subsurface pathways from the subtropical to tropical Atlantic. *J. Phys. Oceanogr.,* **32,** 2257–2276.

Johns, W. E., T. N. Lee, R. C. Beardsley, J. Candela, R. Limeburger, and B. Castro, 1998: Annual cycle and variability of the North Brazil Current. *J. Phys. Oceanogr.,* **28,** 103–128.

Katz, E. J., and S. Garzoli, 1982: Response of the western equatorial Atlantic Ocean to an annual wind cycle. *J. Mar. Res.,* **40** (Suppl.), 307–327.

——, and Coauthors, 1977: Zonal pressure gradient along the equatorial Atlantic. *J. Mar. Res.,* **35,** 293–307.

——, R. L. Molinari, D. E. Cartwright, P. Hisard, H. U. Lass, and A. deMesquita, 1981: The seasonal transport of the Equatorial Undercurrent in the western Atlantic (during the Global Weather Experiment). *Oceanol. Acta,* **4,** 445–450.

Kessler, W. S., G. C. Johnson, and D. W. Moore, 2003: Sverdrup and nonlinear dynamics of the Pacific equatorial currents. *J. Phys. Oceanogr.,* **33,** 994–1008.

Lass, H. U., V. Bubnov, J. M. Huthnance, E. J. Katz, J. Meincke, A. de Mesquita, F. Ostapoff, and B. Voituriez, 1983: Seasonal changes of the zonal pressure gradient in the equatorial Atlantic during the FGGE year. *Oceanol. Acta,* **6,** 3–11.

Lazar, A., T. Inui, P. Malanotte-Rizzoli, A. J. Busalacchi, L. Wang, and R. Murtugudde, 2002: Seasonality of the ventilation of the tropical Atlantic thermocline in an ocean general circulation model. *J. Geophys. Res.,* **107,** 3104, doi:10.1029/2000JC000667.

Liu, Z., 1994: A simple model of the mass exchange between the subtropical and tropical ocean. *J. Phys. Oceanogr.,* **24,** 466–497.

——, and S. G. H. Philander, 1995: How different wind stress patterns affect the tropical subtropical circulations of the upper ocean. *J. Phys. Oceanogr.,* **25,** 449–462.

——, ——, and R. C. Pacanowski, 1994: A GCM study of tropical–subtropical upper-ocean water exchange. *J. Phys. Oceanogr.,* **24,** 2606–2623.

Luyten, J. R., J. Pedlosky, and H. Stommel, 1983: The ventilated thermocline. *J. Phys. Oceanogr.,* **13,** 292–309.

Madec, G., P. Delecluse, M. Imbard, and C. Lévy, 1998: OPA8.1 ocean general circulation model reference manual. Notes du Pôle de Modélisation IPSL, Note 11.

Mayer, D. A., and R. H. Weisberg, 1993: A description of COADS surface meteorological fields and the implied Sverdrup transports for the Atlantic Ocean from 30°S to 60°N. *J. Phys. Oceanogr.,* **23,** 2201–2221.

McCreary, J. P., Jr., and P. Lu, 1994: Interaction between the subtropical and equatorial ocean circulations: The subtropical cell. *J. Phys. Oceanogr.,* **24,** 466–497.

Metcalf, W. G., and M. C. Stalcup, 1967: Origin of the Atlantic Equatorial Undercurrent. *J. Geophys. Res.,* **72,** 4959–4974.

Michel, S., and A.-M. Treguier, 2002: Sensitivity of the Equatorial Undercurrent to mixing parameterisations in the CLIPPER model. Rep. DRO/LPO 02-16, 35 pp.

Pedlosky, J., 1987: An inertial theory of the Equatorial Undercurrent. *J. Phys. Oceanogr.,* **17,** 1978–1985.

——, 1988: Entrainment and the termination of the Equatorial Undercurrent. *J. Phys. Oceanogr.,* **18,** 880–886.

——, 1996: *Ocean Circulation Theory.* Springler-Verlag, 453 pp.

Philander, S. G. H., 1973: Equatorial Undercurrent: Measurements and theories. *Rev. Geophys. Space Phys.,* **11,** 513–570.

——, 1986: Unusual conditions in the tropical Atlantic Ocean in 1984. *Nature,* **322,** 236–238.

——, and R. C. Pacanowski, 1980: The generation of equatorial currents. *J. Geophys. Res.,* **85,** 1123–1136.

——, and ——, 1981: Response of equatorial oceans to periodic forcing. *J. Geophys. Res.,* **86,** 1903–1916.

——, and ——, 1986a: A model of the seasonal cycle in the tropical Atlantic Ocean. *J. Geophys. Res.,* **91,** 14 192–14 206.

——, and ——, 1986b: The mass and heat budget in a model of the tropical Atlantic Ocean. *J. Geophys. Res.,* **91,** 14 212–14 220.

——, and Y. Chao, 1991: On the contrast between the seasonal cycles of the equatorial Atlantic and Pacific Oceans. *J. Phys. Oceanogr.,* **21,** 1399–1406.

——, W. J. Hurlin, and A. D. Seigel, 1987: Simulation of the seasonal cycle of tropical Pacific Ocean. *J. Phys. Oceanogr.,* **17,** 1986–2002.

Provost, C., S. Arnault, N. Chouaib, A. Kartavtseff, L. Bunge, and E. Sultan, 2004: TOPEX-Poseidon and Jason equatorial sea surface slope anomaly in the Atlantic in 2002: Comparison with winds and currentmeter at 23W. *Mar. Geod.,* **27,** 31–45.

Reynaud, T., P. Legrand, H. Mercier, and B. Barnier, 1998: A new analysis of hydrographic data in the Atlantic and its application to an inverse modelling study. *International WOCE Newsletter,* No. 32, WOCE International Project Office, Southampton, United Kingdom, 29–31.

Richardson, P. L., and T. K. McKee, 1984: Average seasonal variation of the Atlantic North Equatorial Countercurrent from ship drift data. *J. Phys. Oceanogr.,* **14,** 1226–1238.

Schott, F. A., and C. W. Böning, 1991: The WOCE model in the western equatorial Atlantic: Upper layer circulation. *J. Geophys. Res.,* **96,** 6993–7004.

——, J. Fischer, and L. Stramma, 1998: Transports and pathways of the upper-layer circulation in the western tropical Atlantic. *J. Phys. Oceanogr.,* **28,** 1904–1928.

——, and Coauthors, 2003: The zonal currents and transports at 35°W in the tropical Atlantic. *Geophys. Res. Lett.,* **30,** 1349, doi:10.1029/2002GL016849.

Stramma, L., and F. Schott, 1999: The mean flow field of the tropical Atlantic Ocean. *Deep-Sea Res. II,* **46,** 279–303.

Thierry, V., A. M. Treguier, and H. Mercier, 2004: Numerical study of the annual and semi-annual fluctuations in the deep equatorial Atlantic ocean. *Ocean Modell.,* **6,** 1–30.

Treguier, A. M., O. Boebel, B. Barnier, and G. Madec, 2003: Agulhas eddy fluxes in a 1/6° Atlantic model. *Deep-Sea Res. II,* **50,** 251–280.

Verdy, A., and M. Jochum, 2005: A note on the validity of the Sverdrup balance in the Atlantic North Equatorial Countercurrent. *Deep-Sea Res. I,* **52,** 179–188.

Wacongne, S., 1989: Dynamical regimes of a fully nonlinear stratified model of the Atlantic Equatorial Undercurrent. *J. Geophys. Res.,* **94,** 4801–4815.

Weisberg, R. H., J. H. Hickman, T. Y. Tang, and T. J. Weingartner, 1987: Velocity and temperature observations during the Seasonal Response of the Equatorial Atlantic Experiment at 0°, 28°W. *J. Geophys. Res.,* **92,** 5061–5075.